Engineering Chemisorption of Fe4 Single-Molecule Magnets on Gold

Lorenzo Poggini, Erik Tancini, Chiara Danieli, Andrea Luigi Sorrentino, Giulia Serrano, Alessandro Lunghi, Luigi Malavolti, Giuseppe Cucinotta, Anne-Laure Barra, Amélie Juhin, Marie-Anne Arrio, Weibin Li, Edwige Otero, Philippe Ohresser, Loïc Joly, Jean Paul Kappler, Federico Totti, Philippe Sainctavit, Andrea Caneschi, Roberta Sessoli, Andrea Cornia,* and Matteo Mannini*

Gaining control over the grafting geometry is critically important for any application of surface-supported single-molecule magnets (SMMs) in data storage, spintronics, and quantum information science. Here, tetrairon(III) SMMs with a propeller-like structure are functionalized with thioacetyl-terminated alkyl chains to promote chemisorption on gold surfaces from solution and to evaluate differences in adsorption geometry and magnetic properties as a function of chain length. The prepared monolayers are investigated using X-ray absorption techniques with linearly and circularly polarized light to extract geometrical and magnetic information, respectively. All derivatives remain intact and form partially oriented monolayers on the gold surface. A ligand-field analysis of the observed X-ray natural linear dichroism shows that the threefold molecular axis is invariably biased toward the surface normal, in agreement with ab initio calculations. This preferential orientation is most pronounced in monolayers of the shortest-chain derivative, which are further studied with an ultralow temperature X-ray magnetic circular dichroism setup operating down to 350 mK. The isothermal field sweeps with the magnetic field at normal incidence show an open hysteresis loop below 1 K, while measurements at different incidence angles prove the magnetic anisotropy of the monolayers.

1. Introduction

Molecules exhibiting a directionally bistable magnetic moment, also known as single-molecule magnets (SMMs),[1–4] have been the target of intense research aimed at exploring their potential use to store information at the molecular level.[5–10] SMMs are mono- or polynuclear coordination compounds of paramagnetic metal ions held together by suitable ligands, which often provide an effective shielding between adjacent molecules in the solid. Most of them feature a combination of a large spin and an easy-axis magnetic anisotropy, which results in a dramatic slowing down of magnetization fluctuations at low temperature and the appearance of magnetic hysteresis.[2,11,12] The temperature values at which the hysteresis is normally observed remain a limit for technological applications,[5–10] but working temperatures above 77 K, the normal boiling point of liquid nitrogen,

L. Poggini, A. L. Sorrentino, G. Serrano, A. Lunghi,[+] L. Malavolti, G. Cucinotta, F. Totti, R. Sessoli, M. Mannini
Department of Chemistry "U. Schiff" – DICUS – and INSTM Research Unit
University of Florence
Via della Lastruccia 3-13, Sesto Fiorentino, FI 50019, Italy
E-mail: matteo.mannini@unifi.it

The ORCID identification number(s) for the author(s) of this article can be found under https://doi.org/10.1002/admi.202101182.

[+]Present address: School of Physics, CRANN Institute and AMBER, Trinity College, Dublin 2, Ireland

L. Poggini, R. Sessoli
Institute for Chemistry of Organo-Metallic Compounds (ICCOM-CNR)
Via Madonna del Piano
Sesto Fiorentino, FI 50019, Italy

E. Tancini, C. Danieli, A. Cornia
Department of Chemical and Geological Sciences and INSTM Research Unit
University of Modena and Reggio Emilia
Via G. Campi 103, Modena 41125, Italy
E-mail: acornia@unimore.it

E. Tancini
Department of Physics, Informatics and Mathematics
University of Modena and Reggio Emilia
Via G. Campi 213/a, Modena 41125, Italy

A. L. Sorrentino, G. Serrano, A. Caneschi
Department of Industrial Engineering – DIEF – and INSTM Research Unit
University of Florence
Via Santa Marta 3, Florence 50139, Italy

A.-L. Barra
Laboratoire National des Champs Magnétiques Intenses
UPR CNRS 3228
Univ. Grenoble-Alpes
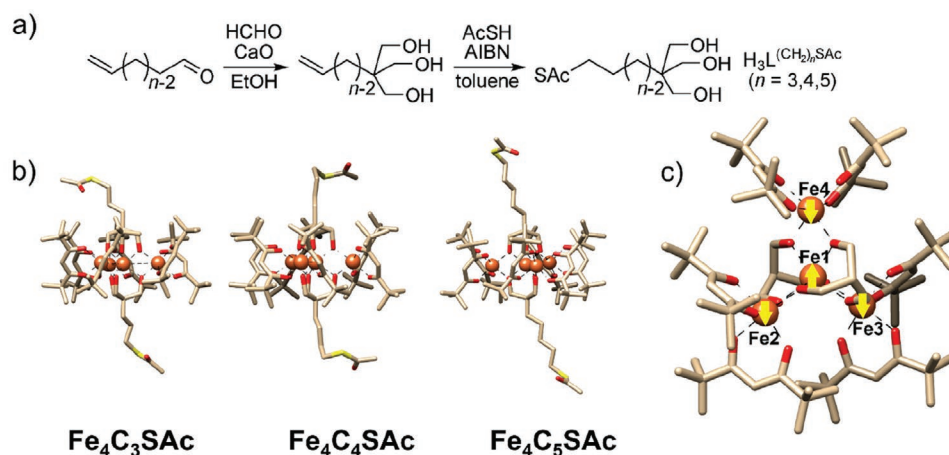25 rue des Martyrs, B.P. 166, Grenoble, Cedex 9 38042, France

ADVANCED
SCIENCE NEWS
www.advancedsciencenews.com

ADVANCED
MATERIALS
INTERFACES
www.advmatinterfaces.de

Figure 1. a) General procedure for the synthesis of the tripodal proligands used in this work; AIBN = 2,2′-azobis(2-methylpropionitrile). b,c) Structure of the investigated Fe_4 derivatives, omitting hydrogen atoms; in c) the R groups are not shown and the yellow arrows represent the arrangement of the iron(III) spins in the $S = 5$ ground state.

have been recently achieved in organometallic complexes containing single dysprosium(III) ions.[13] Other technological applications of SMMs have been proposed based on their rich physics,[14] like exploiting the degrees of freedom of molecular spins in spintronic devices[15–19] and quantum computation.[20–22] To approach these technological targets a crucial step is making SMMs individually accessible while ensuring that they remain structurally and functionally intact. Seminal studies in this direction were performed on propeller-like tetrairon(III) complexes (Fe_4), which possess an $S = 5$ ground state and show SMM behavior at sub-kelvin temperatures.[23] Complexes of this family with the general formula $[Fe_4(L^R)_2(dpm)_6]$ are chemically robust and withstand a variety of processing methods, like solution chemistry and thermal sublimation in ultrahigh vacuum (UHV). In the above formula, Hdpm is dipivaloylmethane and H_3L^R is tripodal proligand 2-R-2-(hydroxymethyl) propane-1,3-diol, which holds the tetrairon(III) core together and carries an R side group.[23] Solution chemistry was used to capture individual Fe_4 molecules in gated metal nanogaps and study the interplay between electron transport and magnetic properties.[24–27] In an alternative approach to single-molecule addressing, Fe_4 complexes were deposited on atomically flat surfaces suitable for scanning probe studies, including Au(111),[9,10,28–32] Cu(100),[32] Cu_2N/Cu(100),[32,33] BN/Rh(111),[34]

graphene/Ir(111),[35,36] and Pb(111).[37] In particular, the investigation of sulfur-functionalized Fe_4 derivatives chemisorbed on Au(111) surface by a wet chemistry approach marked a turning point in the field, as it provided the first sound demonstration that molecule-surface interactions may not critically affect SMM properties.[9,10] These results were subsequently confirmed working on Fe_4 adducts with gold nanoparticles[38] and on physisorbed monolayers prepared by thermal evaporation in UHV.[28,37]

In this respect, it is important to realize that deposition on a native metal substrate is the simplest approach to arrays of individually addressable molecules. However, direct contact with a metal surface was found highly detrimental to the properties of other families of SMMs, like lanthanide double-deckers.[39–41] By contrast, the magnetic bistability of these materials is retained on graphene[42] and on TiO_2 thin layers,[43] and is even enhanced on an Ag(100) surface covered by an ultrathin decoupling layer of MgO.[7,8] The bulky ligand shell of Fe_4 complexes, as the carbon cage of endohedral fullerenes,[5] plays a similar role by effectively shielding the magnetic core from the metallic substrate.

As compared with deposition methods in UHV, chemisorption from solution is operationally simpler and more cost-effective, and produces monolayers of higher stability, though more prone to contamination. Additionally, since chemisorption relies on the formation of specific chemical bonds with the surface, it can be largely controlled by the proper design of the molecular structure.

Chemisorption of Fe_4 complexes on gold was promoted using an R = $(CH_2)_n$SAc side group,[9,10,29–31,44] consisting of a linear alkyl chain terminated by an acetyl-protected thiol function (**Figure 1**).[30,45] As experimentally observed[46,47] and theoretically rationalized,[48,49] these sulfur-containing tethers are expected to undergo spontaneous homolytic cleavage upon adsorption, leading to radical thiols that chemisorb on the surface. The length of the alkyl spacer, as given by the number n of methylene groups, was found to influence the anchoring geometry: while for $n = 9$ the adsorbate is structurally disordered, $n = 5$ results in a partially oriented layer. This last feature

A. Juhin, M.-A. Arrio, W. Li, P. Sainctavit
Institut de Minéralogie, de Physique des Matériaux et de Cosmochimie (IMPMC)
CNRS
Sorbonne Université
4 place Jussieu, Paris, Cedex 5 75252, France

W. Li, E. Otero, P. Ohresser, J. P. Kappler, P. Sainctavit
Synchrotron-SOLEIL
L'Orme des Merisiers
Saint-Aubin 91192, France

L. Joly
Université de Strasbourg
Institut de Physique et Chimie des Matériaux de Strasbourg (IPCMS)
CNRS
UMR 7504, Strasbourg F-67000, France

**ADVANCED
SCIENCE NEWS**

www.advancedsciencenews.com

**ADVANCED
MATERIALS
INTERFACES**

www.advmatinterfaces.de

shows up clearly in the hysteresis loops, which are strongly anisotropic and contain the signature of resonant quantum tunneling processes, one of the key properties of SMMs.[10]

Since SMMs are magnetically anisotropic systems, controlling their orientation on the surface is critically important for applications. In this work, we have explored further shortening of the alkyl spacer's length as a plausible route to enhance preferential orientation. To this aim, we compared the chemisorption geometry and on-surface magnetism of three Fe$_4$ derivatives with $n = 3$, 4, and 5, hereafter indicated as **Fe$_4$C$_n$SAc**, on Au(111).

Cutting-edge experimental work was based on X-ray absorption spectroscopy (XAS) with circular and linear polarization techniques and included ultralow temperature (ULT) measurements. Data interpretation was aided by ligand field multiplet (LFM) calculations and ab initio theoretical modeling, which provided insight into the role played by the spacer's length in the structural and magnetic properties of the monolayers.

2. Results and Discussion

2.1. Synthesis and Bulk Characterization

The tripodal proligands H$_3$L^R used in this work differ in the number ($n = 3$, 4, and 5) of methylene groups in the thioacetyl-terminated alkyl chain R (Figure 1a,b; and Scheme S1, Supporting Information). The derivatives with R = (CH$_2$)$_3$SAc and (CH$_2$)$_4$SAc were synthesized as previously described for the longer chain congeners with $n = 5$[50] and $n = 9$.[45] Such an approach remains in principle feasible for any spacer's length, as long as $n \geq 2$.[51] Tollens condensation[52,53] of the appropriate terminally unsaturated aldehyde with formaldehyde and CaO in ethanol is the key step that affords the metal-chelating trimethylol unit in a one-pot reaction (Figure 1a). The yield of Tollens condensation is limited by the concomitant formation of partially-hydroxylated species along with hemiformals and dehydration byproducts whose separation can be rather difficult.[54–56] The thioacetyl unit is then introduced by the addition of thioacetic acid to the double bond in the presence of a radical initiator like 2,2′-azobis(2-methylpropionitrile) (AIBN) in toluene (Figure 1a).[57,58] In this step, careful control over temperature and reaction time is crucial to achieving high conversions while minimizing the formation of mono- or di-O-acetylated by products. Compounds **Fe$_4$C$_3$SAc**,[59,60] **Fe$_4$C$_4$SAc**, and **Fe$_4$C$_5$SAc**[10] were then synthesized by reacting [Fe$_4$(OMe)$_6$(dpm)$_6$][61] with an excess (2.8–3.1 equivalents) of the appropriate tripodal proligand in Et$_2$O. Although the solubility of the proligands in Et$_2$O gradually decreases with decreasing spacer's length, the reaction proceeds smoothly with all proligands used. The solid material obtained by complete evaporation of the solvent was thoroughly washed with methanol to remove unreacted proligand and recrystallized from anhydrous 1,2-dimethoxyethane to give crystalline tetrairon(III) complexes in 50–60% yield.

The stability of the complexes in dichloromethane was checked by room-temperature ^{1}H-NMR up to 44 h from dissolution (i.e., a timeframe far exceeding that required for the self-assembly process on gold, i.e., 18–20 h). The ^{1}H-NMR spectra show broad signals arising from paramagnetically shifted tBu (10.3 ppm), Ac (2.4–2.5 ppm), and SCH$_2$ (5.0–3.2 ppm) groups.[45] Peaks from the latter are strongly influenced by the chain length, the most downfield-shifted and broadest signal being observed for the shortest-chain derivative, **Fe$_4$C$_3$SAc**. The remaining methylene groups of the ligands are undetectable due to the strong paramagnetism.

All compounds were isolated as air-stable crystalline phases containing no crystallization solvent and suitable for single-crystal X-ray diffraction studies. Careful examination of several crystallization batches revealed the existence of polymorphs of all compounds except **Fe$_4$C$_4$SAc**. Overall, six crystalline phases were characterized (α-**Fe$_4$C$_3$SAc**, β-**Fe$_4$C$_3$SAc**, **Fe$_4$C$_4$SAc**, α-**Fe$_4$C$_5$SAc**, β-**Fe$_4$C$_5$SAc**, and γ-**Fe$_4$C$_5$SAc**) as detailed in Tables S1 and S2 (Supporting Information). The polymorphs differ in the crystal packing, in the conformation of SAc-terminated alkyl chains, and in the ratio between Δ and Λ optical isomers (Figures S1–S3, Supporting Information). Furthermore, β-**Fe$_4$C$_3$SAc** and **Fe$_4$C$_4$SAc** undergo a reversible phase transition around 150–160 K. Except for α-**Fe$_4$C$_5$SAc** (the dominant polymorph of **Fe$_4$C$_5$SAc**) they all crystallize in centrosymmetric space groups, and the crystal is a racemic mixture of Δ and Λ propeller isomers. α-**Fe$_4$C$_5$SAc** crystallizes in noncentrosymmetric space group $P2$ and is not a Δ/Λ racemate, indicating partial spontaneous resolution. More precisely, three of the four crystallographically distinct molecules in the lattice have the same absolute configuration, but different from that of the fourth molecule. A similar case of spontaneous resolution starting from achiral ligands was reported by Saalfrank et al.,[62] while enantiopure tetrairon(III) complexes can be prepared using chiral ligands.[63] All synthesized compounds feature a common tetrairon(III) core displaying either C_2 or C_1 crystallographic symmetry. The core is held together by two bridging (L^R)$^{3-}$ ligands, positioned on either side of the molecular plane, while dpm$^-$ anions provide terminal coordination to peripheral iron(III) centers (Figure 1b,c).[23]

The magnetic behavior of the compounds was investigated by DC and AC magnetic measurements and high-frequency EPR spectra and gave the results presented in Table S3 (Supporting Information). Dominant antiferromagnetic super-exchange interactions between nearest-neighboring high-spin iron(III) centers ($J_1 = 16–17$ cm^{-1} within $J\hat{s}_i \cdot \hat{s}_j$ convention, see the Supporting Information) afford a well-isolated $S = 5$ ground state (Figure 1c), which is subject to quasiaxial zero-field splitting ($D = -0.42$ to -0.43 cm^{-1}). Slow magnetic relaxation is detected at low temperature, with effective barriers $U_{eff}/k_B = 14–15$ K, which are typical for this class of compounds.[23]

2.2. Deposition, Structural, and Magnetic Characterization of the Monolayers

All monolayer samples of **Fe$_4$C$_n$SAc** ($n = 3$, 4, and 5) were prepared in the same way: an Au(111)/mica substrate was incubated in a 2×10^{-3} M solution of the appropriate compound in dichloromethane for 18–20 h and worked out as described in the Supporting Information. XAS at the Fe-L$_{2,3}$ edges was then used to access the electronic structure of the absorbing Fe atoms in the monolayer. All the synchrotron-based experiments reported here were performed at the DEIMOS beamline
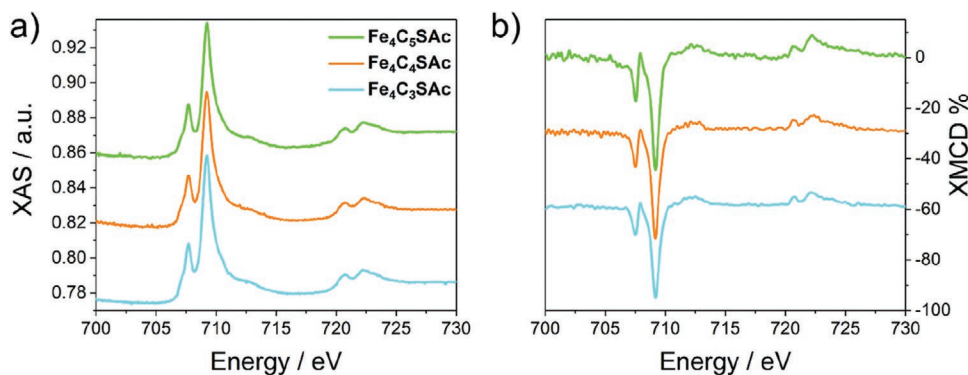
**ADVANCED
SCIENCE NEWS**
www.advancedsciencenews.com

**ADVANCED
MATERIALS
INTERFACES**
www.advmatinterfaces.de

Figure 2. a) Average XAS spectra of **Fe$_4$C$_n$SAc** (n = 3, 4, and 5) recorded at 2.2 K and in an applied field H = 5 T directed at θ = 0° from the surface normal. b) XMCD spectra recorded in the same conditions and normalized to the edge-jump of the average XAS spectrum. A vertical offset was applied for clarity.

at SOLEIL Synchrotron, France.[59,64] XAS is mainly interpreted in the electric dipole approximation, where the cross-section depends only on the nature (circular vs linear) of the X-ray polarization vector and on its orientation with respect to the symmetry axis of the sample.[65] Circularly polarized X-rays allow recording X-ray magnetic circular dichroism (XMCD) signals that provide information on the spin and orbital magnetic moments of the absorbing atom.[66,67] When using linearly polarized X-rays, it is possible to record X-ray natural linear dichroism (XNLD) to get information on structural anisotropies. The average XAS and XMCD spectra of the **Fe$_4$C$_n$SAc** monolayers, presented in **Figure 2**, were recorded at T = 2.2 K by applying an H = 5 T magnetic field at θ = 0° from the surface normal (z). The XMCD spectra were extracted as the difference between the XAS spectra taken with photon helicity polarization antiparallel (σ^-) and parallel (σ^+) to the applied magnetic field, while the average XAS spectra were calculated as $(\sigma^+ + \sigma^-)/2$ (see the Supporting Information, Section Synchrotron characterization). The complete series of XMCD spectra at 2.2 and 4.6 K as a function of θ is reported in Figure S11 (Supporting Information).

In Figure 2a, one can notice that all samples have similar XAS spectral features. The maximum amplitude of the average XAS signal is found at 709.2 eV at the L$_3$ edge. The ratio of the two maxima of the L$_3$ edge (707.6 and 709.2 eV) is ≈1:2.7, consistent with previous measurements on complexes of the same

class in bulk and monolayer forms.[9,10,28–30,35,37,38,68] This indicates that the tetrairon(III) molecules are intact on the surface and that the "3d" electronic structure of the metal core is similar irrespective of the particular tripodal ligand used.

Concerning the XMCD spectra (Figure 2b), the XMCD amplitude is maximum at 709.2 eV and amounts to ≈40% of the average isotropic signal. This value, along with the overall spectral shape and the vanishing XMCD signal at 708.1 eV, is a known fingerprint of the "ferrimagnetic-like" spin arrangement in the ground state of Fe$_4$ complexes (Figure 1c).[69] In Figure S12 (Supporting Information), we report the normalized, XMCD-detected magnetization curves measured for each monolayer, and a trend appears: the XMCD amplitude measured at θ = 0° is invariably larger than that at θ = 45°. This is an indication that the monolayers are magnetically anisotropic with an easy magnetization axis parallel to the surface normal. However, quantitative conclusions about the degree of orientational order in the different samples cannot be inferred from these measurements.

The formation of partially oriented monolayers is most directly revealed by XNLD measurements. **Figure 3** reports the experimental spectra recorded on the same samples studied by XAS and XMCD (Figure 2). The XNLD signal is the difference between XAS cross-sections measured with X-rays having two orthogonal linear polarizations (see the Supporting Information). While cubic molecules have a cross-section that is
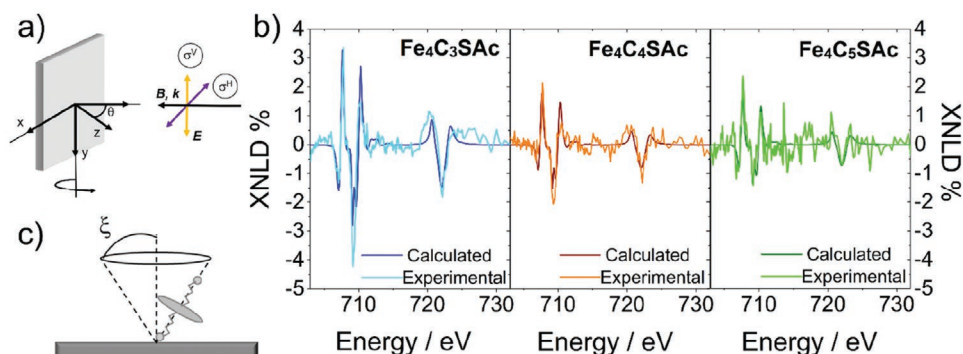

Figure 3. a) Experimental geometry of the XNLD measurements. b) XNLD spectra of monolayers of **Fe$_4$C$_n$SAc** on Au(111) recorded at H = 3 T, θ = 45°, and T = 4 K; XNLD, defined as $\sigma^V - \sigma^H$, is normalized to the average isotropic spectrum (not shown); experimental data are compared with the simulated XNLD spectra based on an angular step distribution at ξ_{MAX} values. c) Sketch of the grafting model for **Fe$_4$C$_n$SAc** complexes.

2101182 (4 of 9)

independent of the direction of the linear polarization vector, Fe_4 molecules are highly anisotropic, with an idealized three-fold axis perpendicular to the metal plane. For an individual molecule, the presence of such threefold axis (at least in a first approximation) implies that electric dipole XAS presents a 2-parameter angular dependence, i.e., all the XNLD signals are homothetic.[65] Again, if such molecules with approximate threefold symmetry were stacked at random with the threefold axis being spherically distributed, there would be no observable XNLD signal. Thus, the observation of an XNLD signal indicates that the molecules are dichroic and that they are not fully orientationally disordered. The two effects cannot be separated from each other because they have the same angular dependence. In the following, we suppose that the electronic charge over surface areas with the size of the X-ray beam (i.e., larger than 100×100 μm²) has cylindrical symmetry, whatever the grafting geometry of the molecules, hence with equivalent x and y directions (Figure 3a).

Thus, a single XNLD measurement with the photon propagation vector **k** at a nonzero angle (here $\theta = 45°$) from z can be used to reveal a preferential orientation along the surface normal. The sizeable XNLD signal detected for all compounds (Figure 3b) is clearly indicative of such preferential ordering. By contrast, monolayers of Fe_4C_9SAc on Au(111) have zero XNLD, as expected from full orientational disorder.[10] Turning now to the spectral profile, it is strikingly similar in the three derivatives, suggesting no gross changes in electronic structure across the series. By analyzing the XNLD signal recorded on monolayers of Fe_4C_5SAc with the aid of LFM calculations, Mannini et al.[10] reproduced the observed profile and, from the XNLD sign, demonstrated that the threefold molecular axis is biased toward the surface normal. Figure 3b shows that a similar situation holds for the whole series, although the magnitude of the XNLD signal significantly increases with decreasing n. In particular, the maximum XNLD amplitude (normalized to the average isotropic XAS spectrum) amounts to ≈2% in Fe_4C_5SAc, is ≈2.5% in Fe_4C_4SAc, and reaches a value as large as 4% in Fe_4C_3SAc. One argues that, as the length of the spacer decreases, preferential orientation is enhanced.

To support this conclusion, we performed LFM calculations[70,71] of the XNLD spectra of the Fe_4C_nSAc series, using the previous analysis of Fe_4C_5SAc for an initial guess of the parameters.[10] The spectrum is the sum of the contributions from the central and the peripheral iron(III) sites. To avoid over-parameterization, axial symmetry was assumed for both ions (see the Supporting Information), as previously adopted

for Fe_4C_5SAc.[10] Moreover, the effect of the 3 T magnetic field applied to improve the S/N ratio was included in the calculation. The chosen set of crystal field parameters (held constant throughout the series, see the Supporting Information) provides a good agreement with the experimental XNLD profile. One can notice that the Dt parameter of the peripheral ions is different from the one used previously,[10] because it was here optimized to improve the matching with the experimental spectral features.

To estimate the extent of preferential orientation, two different model distributions with cylindrical symmetry along z were tested: an angular Gaussian distribution with half-width-at-half-maximum $\xi_{(HWHM)}$ and an angular step distribution with maximum angle ξ_{MAX} (Figure 3c; and Figure S14, Supporting Information). With the former distribution, the XNLD amplitudes recorded on Fe_4C_nSAc monolayers hint at $\xi_{(HWHM)} = 10 \pm 5°$, $31 \pm 2°$, and $34 \pm 2°$ for $n = 3$, 4, and 5, respectively. The use of an angular step distribution, instead, affords $\xi_{MAX} = 10 \pm 5°$, $48 \pm 2°$, and $51 \pm 2°$ for $n = 3$, 4, and 5, respectively (Figure 3b). Thus, a fivefold smaller angle is spanned by the shortest-chain derivative ($n = 3$) as compared with its congeners ($n = 4$ and 5). Both types of angular distributions consistently indicate that orientational ordering is largest in the Fe_4C_3SAc monolayers, while Fe_4C_4SAc and Fe_4C_5SAc behave similarly and display oriented grafting to a significantly lesser extent.

To rationalize the observed behavior for the series, the structure of Fe_4C_nSAc complexes on Au(111) (hereafter indicated as $Fe_4C_nSAc@Au(111)$) was investigated by ab initio molecular dynamics (AIMD). Following the computational protocol developed previously for $Fe_4C_5SAc@Au(111)$,[72] we performed ≈4 ps of AIMD at 200 K for $Fe_4C_3SAc@Au(111)$ and $Fe_4C_4SAc@Au(111)$. The substrate consisted of a four layers slab. Starting from the configuration obtained for $n = 5$,[72] where one aliphatic chain adheres to the surface, the whole system (excluding the bottom layer of the substrate) was let to fully relax. A final geometry optimization on top of a thermal annealing run down to $T \approx 0$ in ≈1 ps was then performed. Comparable geometries to the one computed for $Fe_4C_5SAc@Au(111)$ were obtained.[72] Indeed, for both $n = 3$ and 4 the alkyl chain engaged in the S—Au bond firmly adheres to the gold surface along the entire trajectory (**Figure 4**). The alkyl spacer is then sandwiched between the surface and the disk-like molecular core, which lies roughly parallel to the surface. By consequence, according to AIMD the Fe_4 molecules in the monolayer are partially oriented.

The angle between the surface and the average plane through the metals (ξ) is 24.1° for $n = 3$ and 14.5° for $n = 4$.
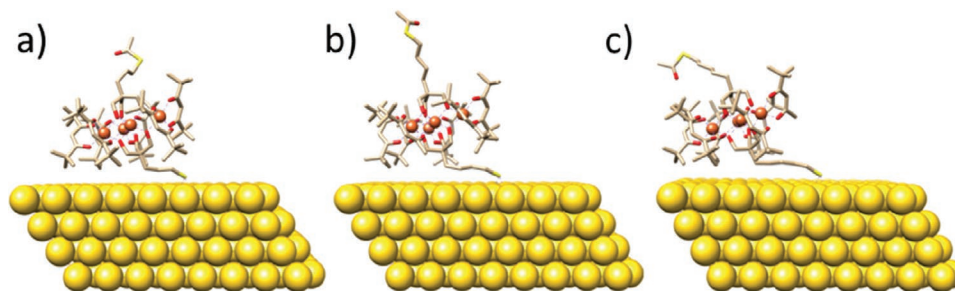

Figure 4. $Fe_4C_nSAc@Au(111)$ model structures for $n = 3$ (a), 4 (b), and 5 (c); hydrogen atoms are not shown for clarity.

Table 1. Isotropic super-exchange couplings (cm^{-1}) in **Fe$_4$C$_n$SAc@Au(111)**.

	$n = 3$	$n = 4$	$n = 5$[a]
J_{12}	10.5	7.2	12.6 (7.8; 17.5)
J_{13}	25.0	22.6	27.1 (16.7; 39.0)
J_{14}	13.5	16.1	23.1 (15.2; 29.7)
J_1[b]	16.3	15.3	21.0 (17.4; 26.9)
J_2[c]	0.1	0.1	0.2 (0.1; 0.2)

[a]Average and extreme values (in parenthesis) computed from the eight AIMD trajectories in ref. [72]; [b]Average n.n. interaction, i.e., $(J_{12}+J_{13}+J_{14})/3$; [c]Next-n.n. interaction (see the Supporting Information for a definition of the super-exchange Hamiltonian used).

Table 2. Magnetic anisotropies (cm^{-1}) and $\xi_{\mathrm{easy\_axis}}$ values (°) obtained for the optimized **Fe$_4$C$_n$SAc@Au(111)** structures after removing the substrate.

	$n = 3$	$n = 4$	$n = 5$[a]
D_1	−1.118	−1.126	−0.789 (−1.177; 1.555)
$|E_1/D_1|$	0.03	0.22	0.17 (0.08; 0.26)
D_2	0.518	0.739	0.565 (0.480; 0.651)
$|E_2/D_2|$	0.15	0.13	0.14 (0.13; 0.16)
D_3	0.418	−0.375	−0.293 (−0.465; 0.536)
$|E_3/D_3|$	0.32	0.19	0.22 (0.14; 0.30)
D_4	0.656	0.557	0.433 (−0.384; 0.747)
$|E_4/D_4|$	0.18	0.18	0.22 (0.14; 0.32)
D	−0.391	−0.380	−0.403 (−0.583; −0.343)
$|E/D|$	0.10	0.03	0.09 (0.02; 0.19)
$\xi_{\mathrm{easy\_axis}}$	16.5	15.5	17.6 (12.2; 36.7)

[a]Average and extreme values (in parenthesis) computed from the eight AIMD trajectories in ref. [72]

Thus, the computed trend for these two derivatives does not match the one extracted from the intensity of the XNLD signal. This is however not surprising, because single trajectory computations provide only partial information on accessible adsorption geometries. A more extensive AIMD study on 8 different trajectories of **Fe$_4$C$_5$SAc@Au(111)** evidenced a wide distribution of conformers spanning a range of geometrical parameters and ξ values (13.9°–18.5°),[72] in agreement with Synchrotron Mössbauer experiments.[44] Therefore, the strong XNLD found for $n = 3$ can be attributed to a reduced possibility for molecules to explore large ξ values in the distribution.

To check the influence of n on the electronic and magnetic properties of adsorbed molecules we computed the most relevant magnetic parameters starting from the optimized geometries. Adsorbed molecules always exhibit C_1 super-exchange symmetry (see **Table 1** and the Supporting Information).[73] The strongest interaction, and the one that is less influenced by the spacer's length, is J_{13} and describes the super-exchange coupling between the central Fe^{3+} ion and the metal center lying approximately above the surface-bound alkyl chain. The other two nearest-neighbor (n.n.) interactions, J_{12} and J_{14}, show more pronounced changes in magnitude and decrease when passing from $n = 5$ to $n = 3$. The average n.n. interaction (J_1) also decreases slightly from $n = 5$ to $n = 3$, whereas J_2, the super-exchange interaction between the peripheral Fe^{3+} ions, is always very small and antiferromagnetic regardless of the spacer's length (Table 1).

The single-ion anisotropy tensors and the overall anisotropy parameters D and E in the $S = 5$ ground state were calculated on the optimized **Fe$_4$C$_n$SAc@Au(111)** structures after removing the substrate. The results are gathered in **Table 2** along with the inclination of the easy magnetic axis in the $S = 5$ ground state with respect to the surface normal ($\xi_{\mathrm{easy\_axis}}$). Notice that $\xi_{\mathrm{easy\_axis}}$ does not necessarily coincide with ξ, since the easy magnetic axis may deviate from the normal to the average plane through the metals. As suggested previously,[44,72] molecule-surface interactions modulate the single-ion anisotropy tensors in magnitude (D_i and E_i) and/or orientation. However, these modifications only marginally influence the ground state D value, which is primarily responsible for the height of the anisotropy barrier and is similar in the three derivatives (Table 2). Although for $n = 3$ and 4 the analysis was based on single trajectory calculations, our theoretical data indicate that the magnetic features of Fe$_4$ SMMs are very robust toward surface-induced deformations even for

short tethers. Therefore, considering both isotropic and anisotropic contributions, all three derivatives are expected to exhibit similar magnetic fingerprints upon adsorption.

Since **Fe$_4$C$_3$SAc** displays the greatest tendency to oriented grafting, a monolayer of this derivative was studied in the mK temperature regime by employing an ULT facility dedicated to soft XMCD experiments (Dichro50), available at DEIMOS beamline (SOLEIL Synchrotron). These data also served to benchmark the end-station.[59] In Figure S13 (Supporting Information), we report the average XAS and XMCD spectra recorded at temperatures between 350 and 900 mK with a magnetic field of 3 T directed along the surface normal.

Figure 5a shows the temperature dependence of the maximum XMCD amplitude at the Fe-L$_3$ edge as a function of the magnetic field. These data highlight the typical magnetic behavior of Fe$_4$ systems, whose hysteresis loops are open below 1 K and become wider with decreasing temperature.[23] The hysteresis curves are almost temperature independent below 0.5 K, indicating the onset of a pure quantum tunneling regime.[37] Magnetization steps due to resonant quantum tunneling are observed at 0 and ±0.5 T; the latter are here clearly visible because of the preferential orientation of the molecules with their easy axis close to the surface normal. Consistent with this, the hysteresis loops are markedly angle-dependent (Figure 5b). As the incidence angle θ increases, saturation is approached more slowly and the magnetization step in nonzero field broadens and shifts to higher fields.[10,28]

3. Conclusions

Here we described a detailed study on 2D arrays of tetrairon(III) SMMs with a propeller-like structure and (CH$_2$)$_n$SAc tethers of different length ($n = 3$, 4, and 5). The molecules were deposited on Au(111) from solution and the resulting self-assembled monolayers were probed by highly surface sensitive techniques based on synchrotron radiation, namely XAS, XMCD, and XNLD. XAS and XMCD provided compelling
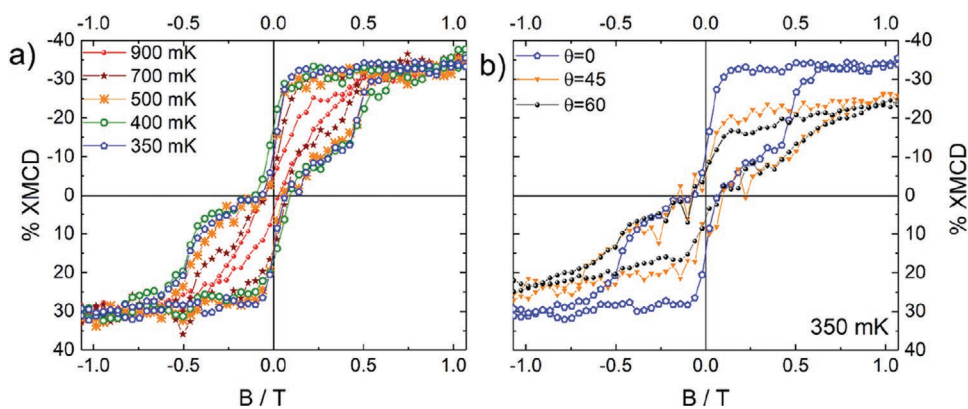
Figure 5. a) XMCD-detected hysteresis loops of a monolayer of **Fe$_4$C$_3$SAc** on Au(111) recorded in the 350–900 mK range at $\theta = 0°$ and with a field sweep rate of 0.01 T s^{-1}. b) Angular dependence of the hysteresis loops for $\theta = 0°$, 45°, and 60° at the same base temperature (350 mK).

evidences that molecules remain structurally intact and maintain their magnetic properties on the surface, consistent with the results of AIMD calculations. According to XNLD, all monolayers exhibit a significant structural anisotropy which was analyzed by LFM calculations. The results showed that the anisotropic signal arises from a partially oriented grafting of the molecules whose idealized threefold axis is biased toward the surface normal. The derivative with the shortest alkyl spacer ($n = 3$) exhibits the most pronounced oriented grafting in the series; its XMCD-detected hysteresis loops, measured down to 350 mK, are markedly dependent on the magnetic field incidence angle and, for normal incidence, display pronounced quantum tunneling steps.

These results confirm that Fe$_4$ SMMs carrying (CH$_2$)$_n$SAc groups form chemisorbed monolayers of structurally and functionally intact molecules on Au(111) for a wide range of n values. However, the structural and magnetic properties of the monolayers are sensitive to the length of the tethering units, which influences the grafting geometry and the shape of the hysteresis loops.

Supporting Information

Supporting Information is available from the Wiley Online Library or from the author.

Acknowledgements

Conflict of Interest

The authors declare no conflict of interest.

Author Contributions

Data Availability Statement

Research data are not shared.

Keywords

[1] A. Caneschi, D. Gatteschi, R. Sessoli, A. L. Barra, L. C. Brunel, M. Guillot, *J. Am. Chem. Soc.* **1991**, *113*, 5873.

[2] R. Sessoli, D. Gatteschi, A. Caneschi, M. A. Novak, *Nature* **1993**, *365*, 141.

ADVANCED
SCIENCE NEWS
www.advancedsciencenews.com

ADVANCED
MATERIALS
INTERFACES
www.advmatinterfaces.de

[3] D. Gatteschi, R. Sessoli, J. Villain, *Molecular Nanomagnets*, Oxford University Press, Oxford **2006**.

[4] A. Zabala-Lekuona, J. M. Seco, E. Colacio, *Coord. Chem. Rev.* **2021**, *441*, 213984.

[5] C. Chen, L. Spree, E. Koutsouflakis, D. S. Krylov, F. Liu, A. Brandenburg, G. Velkos, S. Schimmel, S. M. Avdoshenko, A. Fedorov, E. Weschke, F. Choueikani, P. Ohresser, J. Dreiser, B. Büchner, A. A. Popov, *Adv. Sci.* **2021**, *8*, 2000777.

[6] F. Paschke, T. Birk, V. Enenkel, F. Liu, V. Romankov, J. Dreiser, A. A. Popov, M. Fonin, *Adv. Mater.* **2021**, *33*, 2102844.

[7] M. Studniarek, C. Wäckerlin, A. Singha, R. Baltic, K. Diller, F. Donati, S. Rusponi, H. Brune, Y. Lan, S. Klyatskaya, M. Ruben, A. P. Seitsonen, J. Dreiser, *Adv. Sci.* **2019**, *6*, 1901736.

[8] C. Wäckerlin, F. Donati, A. Singha, R. Baltic, S. Rusponi, K. Diller, F. Patthey, M. Pivetta, Y. Lan, S. Klyatskaya, M. Ruben, H. Brune, J. Dreiser, *Adv. Mater.* **2016**, *28*, 5195.

[9] M. Mannini, F. Pineider, P. Sainctavit, C. Danieli, E. Otero, C. Sciancalepore, A. M. Talarico, M.-A. Arrio, A. Cornia, D. Gatteschi, R. Sessoli, *Nat. Mater.* **2009**, *8*, 194.

[10] M. Mannini, F. Pineider, C. Danieli, F. Totti, L. Sorace, P. Sainctavit, M.-A. Arrio, E. Otero, L. Joly, J. C. Cezar, A. Cornia, R. Sessoli, *Nature* **2010**, *468*, 417.

[11] L. Thomas, F. Lionti, R. Ballou, D. Gatteschi, R. Sessoli, B. Barbara, *Nature* **1996**, *383*, 145.

[12] A. Cornia, A. C. Fabretti, P. Garrisi, C. Mortalò, D. Bonacchi, D. Gatteschi, R. Sessoli, L. Sorace, W. Wernsdorfer, A. L. Barra, *Angew. Chem., – Int. Ed.* **2004**, *43*, 1136.

[13] F.-S. Guo, B. M. Day, Y.-C. Chen, M.-L. Tong, A. Mansikkamäki, R. A. Layfield, *Science* **2018**, *362*, 1400.

[14] E. Moreno-Pineda, W. Wernsdorfer, *Nat. Rev. Phys.* **2021**, *3*, 645.

[15] A. R. Rocha, V. M. García-Suárez, S. W. Bailey, C. J. Lambert, J. Ferrer, S. Sanvito, *Nat. Mater.* **2005**, *4*, 335.

[16] L. Bogani, W. Wernsdorfer, *Nat. Mater.* **2008**, *7*, 179.

[17] A. Candini, S. Klyatskaya, M. Ruben, W. Wernsdorfer, M. Affronte, *Nano Lett.* **2011**, *11*, 2634.

[18] M. Urdampilleta, S. Klyatskaya, J. P. Cleuziou, M. Ruben, W. Wernsdorfer, *Nat. Mater.* **2011**, *10*, 502.

[19] G. Cucinotta, L. Poggini, F. Bertani, N. Cristiani, M. Torelli, P. Graziosi, I. Cimatti, B. Cortigiani, E. Otero, R. Sessoli, M. Mannini, P. Ohresser, P. Sainctavit, A. Dediu, E. Dalcanale, R. Sessoli, M. Mannini, *Adv. Funct. Mater.* **2017**, *27*, 1703600.

[20] M. N. Leuenberger, D. Loss, *Nature* **2001**, *410*, 789.

[21] A. Palii, B. Tsukerblat, J. M. Clemente-Juan, A. Gaita-Ariño, E. Coronado, *Phys. Rev. B* **2011**, *84*, 184426.

[22] C. Godfrin, A. Ferhat, R. Ballou, S. Klyatskaya, M. Ruben, W. Wernsdorfer, F. Balestro, *Phys. Rev. Lett.* **2017**, *119*, 187702.

[23] A. Cornia, M. Mannini, R. Sessoli, D. Gatteschi, *Eur. J. Inorg. Chem.* **2019**, *2019*, 552.

[24] M. Misiorny, E. Burzurí, R. Gaudenzi, K. Park, M. Leijnse, M. R. Wegewijs, J. Paaske, A. Cornia, H. S. J. van der Zant, *Phys. Rev. B* **2015**, *91*, 035442.

[25] E. Burzurí, R. Gaudenzi, H. S. J. van der Zant, *J. Phys. Condens. Matter* **2015**, *27*, 113202.

[26] N. Gallego-Planas, A. Martín-Rodríguez, E. Ruiz, *Dalton Trans.* **2016**, *45*, 18867.

[27] F.-X. Zu, G.-Y. Gao, H.-H. Fu, L. Xiong, S.-C. Zhu, L. Peng, K.-L. Yao, *Appl. Phys. Lett.* **2015**, *107*, 252403.

[28] L. Malavolti, V. Lanzilotto, S. Ninova, L. Poggini, I. Cimatti, B. Cortigiani, L. Margheriti, D. Chiappe, E. Otero, P. Sainctavit, F. Totti, A. Cornia, M. Mannini, R. Sessoli, *Nano Lett.* **2015**, *15*, 535.

[29] R. Sessoli, M. Mannini, F. Pineider, A. Cornia, P. Sainctavit, in *Magnetism and Synchrotron Radiation* (Eds: E. Beaurepaire, H. Bulou, F. Scheurer, J. P. Kappler), Springer Proc. Phys., Vol. *133*, Springer, **2010**, pp. 279–311.

[30] P. Totaro, L. Poggini, A. Favre, M. Mannini, P. Sainctavit, A. Cornia, A. Magnani, R. Sessoli, *Langmuir* **2014**, *30*, 8645.

[31] F. Pineider, M. Mannini, C. Danieli, L. Armelao, F. M. Piras, A. Magnani, A. Cornia, R. Sessoli, *J. Mater. Chem.* **2010**, *20*, 187.

[32] V. Lanzilotto, L. Malavolti, S. Ninova, I. Cimatti, L. Poggini, B. Cortigiani, M. Mannini, F. Totti, A. Cornia, R. Sessoli, *Chem. Mater.* **2016**, *28*, 7693.

[33] J. A. J. Burgess, L. Malavolti, V. Lanzilotto, M. Mannini, S. Yan, S. Ninova, F. Totti, S. Rolf-Pissarczyk, A. Cornia, R. Sessoli, S. Loth, *Nat. Commun.* **2015**, *6*, 8216.

[34] P. Erler, P. Schmitt, N. Barth, A. Irmler, S. Bouvron, T. Huhn, U. Groth, F. Pauly, L. Gragnaniello, M. Fonin, *Nano Lett.* **2015**, *15*, 4546.

[35] L. Gragnaniello, F. Paschke, P. Erler, P. Schmitt, N. Barth, S. Simon, H. Brune, S. Rusponi, M. Fonin, *Nano Lett.* **2017**, *17*, 7177.

[36] F. Paschke, P. Erler, V. Enenkel, L. Gragnaniello, M. Fonin, *ACS Nano* **2019**, *13*, 780.

[37] G. Serrano, L. Poggini, M. Briganti, A. L. Sorrentino, G. Cucinotta, L. Malavolti, B. Cortigiani, E. Otero, P. Sainctavit, S. Loth, F. Parenti, A.-L. Barra, A. Vindigni, A. Cornia, F. Totti, M. Mannini, R. Sessoli, *Nat. Mater.* **2020**, *19*, 546.

[38] M. Perfetti, F. Pineider, L. Poggini, E. Otero, M. Mannini, L. Sorace, C. Sangregorio, A. Cornia, R. Sessoli, *Small* **2014**, *10*, 323.

[39] L. Malavolti, L. Poggini, L. Margheriti, D. Chiappe, P. Graziosi, B. Cortigiani, V. Lanzilotto, F. B. B. de Mongeot, P. Ohresser, E. Otero, F. Choueikani, P. Sainctavit, I. Bergenti, V. A. A. Dediu, M. Mannini, R. Sessoli, *Chem. Commun.* **2013**, *49*, 11506.

[40] A. Lodi Rizzini, C. Krull, A. Mugarza, T. Balashov, C. Nistor, R. Piquerel, S. Klyatskaya, M. Ruben, P. M. Sheverdyaeva, P. Moras, C. Carbone, C. Stamm, P. S. Miedema, P. K. Thakur, V. Sessi, M. Soares, F. Yakhou-Harris, J. C. Cezar, S. Stepanow, P. Gambardella, *Surf. Sci.* **2014**, *630*, 361.

[41] S. Stepanow, J. Honolka, P. Gambardella, L. Vitali, N. Abdurakhmanova, T.-C. Tseng, S. Rauschenbach, S. L. Tait, V. Sessi, S. Klyatskaya, M. Ruben, K. Kern, *J. Am. Chem. Soc.* **2010**, *132*, 11900.

[42] G. Serrano, E. Velez-Fort, I. Cimatti, B. Cortigiani, L. Malavolti, D. Betto, A. Ouerghi, N. B. Brookes, M. Mannini, R. Sessoli, *Nanoscale* **2018**, *10*, 2715.

[43] A. L. Sorrentino, I. Cimatti, G. Serrano, L. Poggini, B. Cortigiani, L. Malavolti, E. Otero, P. Sainctavit, M. Mannini, R. Sessoli, A. Caneschi, *J. Mater. Chem. C* **2021**, https://doi.org/10.1039/D1TC03408A.

[44] A. Cini, M. Mannini, F. Totti, M. Fittipaldi, G. Spina, A. Chumakov, R. Rüffer, A. Cornia, R. Sessoli, *Nat. Commun.* **2018**, *9*, 480.

[45] A.-L. Barra, F. Bianchi, A. Caneschi, A. Cornia, D. Gatteschi, L. Gorini, L. Gregoli, M. Maffini, F. Parenti, R. Sessoli, L. Sorace, A. M. Talarico, *Eur. J. Inorg. Chem.* **2007**, *2007*, 4145.

[46] R. Ghanbaripour, I. Mohammadpoor-Baltork, M. Moghadam, A. R. Khosropour, S. Tangestaninejad, V. Mirkhani, *Polyhedron* **2012**, *31*, 721.

[47] M. I. Béthencourt, L. Srisombat, P. Chinwangso, T. R. Lee, *Langmuir* **2009**, *25*, 1265.

[48] G. Rajaraman, A. Caneschi, D. Gatteschi, F. Totti, *Phys. Chem. Chem. Phys.* **2011**, *13*, 3886.

[49] M. Jaccob, G. Rajaraman, F. Totti, *Theor. Chem. Acc.* **2012**, *131*, 1150.

[50] E. Tancini, M. Mannini, P. Sainctavit, E. Otero, R. Sessoli, A. Cornia, *Chem. – Eur. J.* **2013**, *19*, 16902.

[51] A. Cornia, C. Danieli, F. Meglioli, E. Tancini, A. Nicolini, M. J. Rodriguez-Douton, A.-L. Barra, M. Affronte, R. Sessoli, *Magnetochemistry* **2020**, *6*, 55.

[52] B. Tollens, P. Wiegand, *Liebigs Ann. Chem.* **1891**, *265*, 316.

[53] O. C. Dermer, P. W. Solomon, *J. Am. Chem. Soc.* **1954**, *76*, 1697.

[54] T. J. Dunn, W. L. Neumann, M. M. Rogic, S. R. Woulfe, *J. Org. Chem.* **1990**, *55*, 6368.

[55] M. G. Dupont, R. Dulou, A. Duplessis-Kergomard, *Bull. Soc. Chim. Fr.* **1949**, *5*, 314.

[56] A. Muth, A. Asam, G. Huttner, A. Barth, L. Zsolnai, *Chem. Ber.* **1994**, *127*, 305.

[57] K. Motesharei, D. C. Myles, *J. Am. Chem. Soc.* **1997**, *119*, 6674.

[58] V. Gagnard, A. Leydet, A. Morère, J.-L. Montero, I. Lefèbvre, G. Gosselin, C. Pannecouque, E. De Clercq, *Bioorg. Med. Chem.* **2004**, *12*, 1393.

[59] J.-P. Kappler, E. Otero, W. Li, L. Joly, G. Schmerber, B. Muller, F. Scheurer, F. Leduc, B. Gobaut, L. Poggini, G. Serrano, F. Choueikani, E. Lhotel, A. Cornia, R. Sessoli, M. Mannini, M.-A. Arrio, P. Sainctavit, P. Ohresser, *J. Synchrotron Radiat.* **2018**, *25*, 1727.

[60] A. Cornia, A.-L. Barra, G. Poneti, E. Tancini, R. Sessoli, *J. Magn. Magn. Mater.* **2020**, *510*, 166713.

[61] S. Accorsi, A. L. Barra, A. Caneschi, G. Chastanet, A. Cornia, A. C. Fabretti, D. Gatteschi, C. Mortalo, E. Olivieri, F. Parenti, P. Rosa, R. Sessoli, L. Sorace, W. Wernsdorfer, L. Zobbi, *J. Am. Chem. Soc.* **2006**, *128*, 4742.

[62] R. W. Saalfrank, I. Bernt, M. M. Chowdhry, F. Hampel, G. B. M. Vaughan, *Chem. – Eur. J.* **2001**, *7*, 2765.

[63] J. Mayans, M. Font-Bardia, A. Escuer, *Dalton Trans.* **2018**, *47*, 8392.

[64] P. Ohresser, E. Otero, F. Choueikani, K. Chen, S. Stanescu, F. Deschamps, T. Moreno, F. Polack, B. Lagarde, J.-P. Daguerre, F. Marteau, F. Scheurer, L. Joly, J.-P. Kappler, B. Muller, O. Bunau, P. Sainctavit, *Rev. Sci. Instrum.* **2014**, *85*, 013106.

[65] C. Brouder, *J. Phys.: Condens. Matter* **1990**, *2*, 701.

[66] B. Thole, P. Carra, F. Sette, G. van der Laan, *Phys. Rev. Lett.* **1992**, *68*, 1943.

[67] P. Carra, B. T. Thole, M. Altarelli, X. Wang, *Phys. Rev. Lett.* **1993**, *70*, 694.

[68] M. Mannini, F. Pineider, P. Sainctavit, L. Joly, A. Fraile-Rodríguez, M.-A. Arrio, C. Cartier dit Moulin, W. Wernsdorfer, A. Cornia, D. Gatteschi, R. Sessoli, *Adv. Mater.* **2009**, *21*, 167.

[69] M. Mannini, E. Tancini, L. Sorace, P. Sainctavit, M.-A. Arrio, Y. Qian, E. Otero, D. Chiappe, L. Margheriti, J. C. Cezar, R. Sessoli, A. Cornia, *Inorg. Chem.* **2011**, *50*, 2911.

[70] F. M. F. de Groot, J. C. Fuggle, B. T. Thole, G. A. Sawatzky, *Phys. Rev. B* **1990**, *42*, 5459.

[71] B. T. Thole, G. van der Laan, J. C. Fuggle, G. A. Sawatzky, R. C. Karnatak, J.-M. Esteva, *Phys. Rev. B* **1985**, *32*, 5107.

[72] A. Lunghi, M. Iannuzzi, R. Sessoli, F. Totti, *J. Mater. Chem. C* **2015**, *3*, 7294.

[73] A. Lunghi, F. Totti, *J. Mater. Chem. C* **2014**, *2*, 8333.